Surface & Coatings Technology 526 (2026) 133364

Contents lists available at ScienceDirect

Surface & Coatings Technology

journal homepage: www.elsevier.com/locate/sct

In-situ analysis of metal atom, metal ion and argon ion fluxes in industrial magnetron sputtering with Al, Cr and AlCr targets☆

Peter Klein [a], Jaroslav Hnilica [a], Mojmír Jílek [b], Mayur Khan [c], Anna Macková [c], Petr Vašina [a,*]

[a] Department of Plasma Physics and Technology, Masaryk University, Kotlářská 2, CZ-61137, Brno, Czech Republic
[b] SHM, s.r.o., Průmyslová 3020/3, Šumperk 78701, Czech Republic
[c] Nuclear Physics Institute of the Czech Academy of Sciences, Rez, 250 68, Czech Republic

ARTICLE INFO

Keywords:
Magnetron sputtering
DCMS
Industry
Coatings
IMFF
QCM

ABSTRACT

This paper presents a study on the measurement of particle fluxes (Al, Al^+, Cr, Cr^+, Ar^+) at the substrate position during magnetron sputtering deposition. The fluxes were investigated for pure aluminium and chromium targets, as well as their alloy. The industrial magnetron deposition system employs a novel focused magnetron sputtering technique, where only a small portion of the cylindrical target is sputtered at a given time because the plasma is confined to a narrow ring enclosing the target and, thanks to movable magnets, periodically moves over the entire length of the cylinder. This arrangement enables very high power densities (~625 $W.cm^{-2}$) to be achieved using a continuous direct current power supply. Using a biasable quartz crystal microbalance system, both atomic and ionic fluxes of the metal particles were quantified. The same system, configured as a flat Langmuir probe in a saturated ion flux region, was also used to measure the total ion flux. To differentiate between the aluminium and chromium fluxes sputtered from the alloy target, Rutherford backscattering spectrometry of the deposited samples was used. This pioneering approach enables the quantification and differentiation of atomic and ionic species of film-forming elements, as well as the argon ion flux, which are critical parameters in thin-film deposition. Despite the ionised metal flux fraction of the sputtered species reaching around 15%, the flux of metal ions on the substrate is ten times lower than that of argon ions.

1. Introduction

The ionisation of sputtered species during thin film deposition using magnetron sputtering significantly influences the quality and properties of the resulting thin films. Ionised species enhance the adhesion of the thin film to the substrate [1] and help deposit a more compact and dense structure with reduced porosity [2–4]. This leads to improved mechanical properties such as hardness and wear resistance [5,6]. Additionally, ion bombardment contributes to achieving a smoother surface [7–9]. The energy and flux of the ionised species can be controlled to manage the residual stress within the thin film, the film's composition, microstructure, and texture [10–14], enabling customisation for specific applications such as protective coatings [15–17], optical coatings [18,19], and semiconductor devices [20,21]. Overall, the ionisation of sputtered species is a critical factor in producing high-quality thin films with desirable properties for various industrial applications. Therefore, achieving the highest possible ionisation is highly desirable.

The ionisation of the sputtered species can be determined utilising a biasable quartz crystal microbalance (QCM) system, from which the ionised metal flux fraction (IMFF) is derived. The biasable QCM was employed to investigate ionisation in the laboratory system for wide range of single elements such as Al [22,23], C [22,23], Cu [24–27], Cr [28], Fe [29], Ni [30] and Ti [23,30–35]. Recently, the biasable QCM was successfully used in the industrial environment to investigate ionisation of direct current magnetron sputtering (DCMS) for Al, Cr and Ti targets [36], DCMS enhanced by large-volume lateral arc discharge using Ti target [37] as well as focused magnetron sputtering using Ti target [38].

The use of alloy targets in magnetron sputtering offers several advantages over single-element targets. By providing a fixed elemental ratio, alloy targets enable the deposition of films with uniform

☆ This article is part of a Special issue entitled: 'TACT2025' published in Surface & Coatings Technology.

* Corresponding author.
E-mail address: vasina@physics.muni.cz (P. Vašina).

https://doi.org/10.1016/j.surfcoat.2026.133364
Received 31 December 2025; Received in revised form 19 February 2026; Accepted 6 March 2026
Available online 7 March 2026

Table 1
Discharge characteristics in an industrial system. The racetrack area is about 40 cm^2.

p	P	P/S	Al			Cr			AlCr alloy		
(Pa)	(kW)	(W cm^{-2})	U (V)	I (A)	j (mA cm^{-2})	U (V)	I (A)	j (mA cm^{-2})	U (V)	I (A)	j (mA cm^{-2})
0.28	5	125	432	11.5	288	394	12.8	320	361	13.9	348
0.28	10	250	422	23.8	595	405	24.7	618	357	28.0	700
0.28	15	375	427	35.2	880	417	36.4	910	357	42.3	1058
0.28	20	500	447	44.7	1118	437	45.8	1145	362	54.4	1360
0.28	25	625	483	51.9	1298	470	53.3	1333	–	–	–
0.52	20	500	440	45.4	1135	420	47.7	1193	355	56.4	1410
0.98	20	500	440	45.4	1135	410	48.9	1223	347	57.3	1433

and reproducible composition. In contrast, co-sputtering from separate elemental targets often introduces compositional variations, as differences in sputtering yields cause uneven erosion rates [39], leading to stoichiometric drift in the growing film. Employing a single alloy cathode enhances plasma stability and simplifies scaling, enabling a smoother transition from laboratory-scale experiments to industrial applications [40]. Moreover, alloy targets simplify the sputtering setup by eliminating the need to independently regulate multiple magnetrons or power supplies. This reduction in system complexity is particularly advantageous for industrial-scale and long-duration coating processes.

Metal ions play a crucial role in enhancing the properties of thin films. However, each metal has different ionisation cross-sections and ionisation potentials [41]. Therefore, it is essential to understand which elements are more likely to be ionised and which may be more susceptible to back-attraction, a phenomenon observed in high-power impulse magnetron sputtering (HiPIMS) [42,43]. To evaluate the behaviour of various metals, both individually and in alloys, under industrial conditions, QCM measurements were utilised.

2. Experimental

2.1. Industrial sputtering system

Fig. 1 shows a schematic drawing of the physical vapour deposition (PVD) unit DRAK developed by SHM s.r.o., Šumperk, Czech Republic [44]. The chamber with dimensions 580 L × 650 W × 705 H (mm) is evacuated to a base pressure below 9×10^{-3} Pa with a tandem assembly of Pfeiffer Hena 41 rotary and Pfeiffer HiPace 700M turbo-molecular pumps. Argon gas is introduced from the top of the chamber over MKS 500 sccm flow meter and the working pressure is measured using the MKS 627F Baratron gauge. The carousel substrate holder is capable of rotating in three planetary rotation axes around the magnetron cathode situated in the centre of the chamber. The system utilises a rotating cylindrical cathode equipped with a cylindrical target 50 cm long, 10 cm in diameter and 1 cm thick. For this study, a novel coating deposition technology called moving focused magnetic field magnetron sputtering (F-MS) [38,45] is used. In F-MS, the magnet arrangement creates a 40 cm^2 ring-shaped erosion zone (racetrack) sputtering particles around the 360-degree circumference of the ring. To sputter over the entire length of the cathode, the magnets within a cylindrical target are moved periodically along the entire length of the cathode with a frequency of 1.2 Hz. Throughout the experiments, three distinct materials were sputtered from a rotating cylindrical target: aluminium, chromium and AlCr alloy (60:40). The magnetron cathode is supplied with power up to 25 kW by a TruPlasma DC 4040 (G2) DC generator manufactured by TRUMPF Hüttinger. Such high power delivery is only possible due to the highly efficient cooling of tubular targets [46]. The discharge conditions used in this paper are typical for an industrial process, all are summarised in Table 1.

2.2. Biasable quartz crystal microbalance

A biasable quartz crystal microbalance system was utilised to measure the flux of metal atoms and ions, from which the ionised metal flux fraction was derived as the ratio of metal ions flux to the sum of metal ion and metal atom fluxes [47]. For measurement, the rotation of the substrate holder was stopped and the whole carousel was kept on the ground potential. The QCM system consisted of two Inficon FTM-2400 sensors placed on one substrate holder, 14 cm from the middle of the magnetron cathode directly facing it. One sensor in the QCM system was standard, collecting both atomic and ionic fluxes of the film-forming species, while the second sensor was positively biased by 30 V to repulse positive ions [48] and measured only the atom flux of film-forming species. The biasable QCM sensor was shielded from enhanced electron bombardment by placing it into the metal box with a measurement window, where a metal grid was situated, and the whole encasing was kept at ground potential. This ensured that no parasitic discharge was created on the biased QCM and that the surface potential (outside the sensor itself) was the same as the rest of the substrate. Note that the measured flux of the metal species must be corrected for the transmittance of a grid [37], which was obtained during the calibration process when both QCM sensors were kept at the ground potential. Additional details about biasable QCM measurements can be found in the literature [29–31].

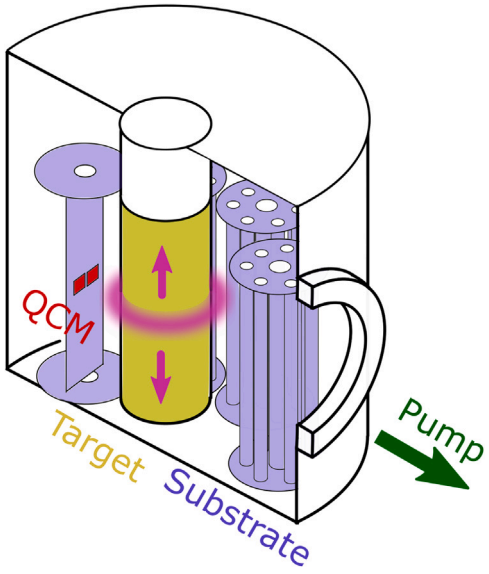

Fig. 1. Schematics of the industrial system with the indicated position of the biased QCM. The pink areas represent the discharge in front of the magnetron cathode.

The eigenfrequency of the quartz crystal within the QCM sensor changes as the film is being deposited onto its surface. This frequency change is proportional to the mass that has been deposited. Thus, the data were recalculated to obtain particle flux (both atomic and ionic) and the results for each target material could be compared. More details can be found in the previous manuscript [34].

For the quality of the growing film, even a bombardment by non-reactive argon ions is essential [49,50]. The biasable QCM allows it to

be reconfigured to essentially work as a flat Langmuir probe. For the experiments, a biasable QCM equipped with the grid was used, and the grid transmissivity for the argon ions is assumed to be the same as for the metal ions; therefore, the same grid correction factor was applied. As the surface of the crystal exposed to the deposition is biased by -50 V, all electrons are repulsed and the current flowing through the crystal is equal to the saturated ion current. This current is measured as a voltage drop induced on 470 Ω resistor and captured by a 1/10 differential probe connected to the Rigol MSO5104 oscilloscope. If only single-charged ions are considered in the discharge, the Langmuir probe regime provides overall ionic flux, while biased QCM provides metallic flux. Subtracting metallic flux thus allows the calculation of the argon ion flux [35].

2.3. Coating deposition and analysis

Si (100) wafers, cut into 1 × 1.5 cm pieces, were used as substrates. They were first ultrasonicated for 1 min in an acetone bath, followed by another 1 min in an isopropanol bath. The samples were then mounted on a motorised substrate holder, positioned 14 cm from the middle of the magnetron cathode, directly facing it — identical to the QCM positioning with metal grid. The substrates were either grounded or biased to 30 V to replicate the QCM conditions. No intentional heating was applied, and each deposition lasted 10 min.

The chemical composition of the coatings was analysed using ion beam analytical techniques, specifically Rutherford Back-scattering spectrometry (RBS) and elastic recoil detection analysis (ERDA), employing the tandem accelerator Tandetron MC 4130 at the Nuclear Physics Institute in Řež near Prague. In the RBS experiments, beams of H^+ and He^+ ions were utilised at several discrete energies: 1.74 MeV, which provides enhanced sensitivity for carbon; 2.0 MeV; 2.5 MeV, measured simultaneously with ERDA; 3.07 MeV, offering improved sensitivity for oxygen; and 3.72 MeV, which is particularly effective for nitrogen analysis. The choice of these energies was motivated by the presence of resonant scattering cross sections that significantly enhance the detection sensitivity for light elements such as carbon and nitrogen. The scattered ions emerging from the sample were detected using an ORTEC ULTRA-series silicon detector, featuring an active area of 50 mm^2 and a depletion layer thickness of 300 μm. The detector was positioned at a scattering angle of 170°, with a slight offset of 10° out of the plane, to optimise the collection of backscattered particles. For ERDA measurements, 2.5 MeV He ions were employed at an incident angle of 75°, corresponding to a scattering angle of 30°. To suppress the detection of lighter recoiled particles and ensure selective measurement of heavier ions, the detector was covered with a 12 μm thick PET foil. The overall energy resolution of the detection system was determined to be 25 keV, sufficient to resolve elemental contributions in the thin film samples under investigation.

This experimental configuration, combining RBS and ERDA, allowed for a comprehensive characterisation of the elemental composition and depth profiles of the studied materials. The use of resonant RBS energies provided enhanced sensitivity for light elements, particularly carbon and nitrogen, which are otherwise challenging to quantify due to their low scattering cross sections under purely Rutherford conditions. By exploiting these resonances, the accuracy and reliability of the compositional analysis were significantly improved, enabling precise determination of stoichiometry and impurity levels in the investigated samples.

2.4. Determination of individual element ionisation in the deposition of AlCr alloy

To determine fluxes of the individual elements sputtered from the AlCr alloy, one has to differentiate them separately from the QCM measurement. For this task, a motorised biasable substrate holder equipped with the same grid as the biasable QCM assembly was used to deposit thin films under the same deposition conditions as the biasable QCM was measuring. Because of the very high deposition rate of the *F*-MS, the deposition took only a few minutes. After deposition, the atomic composition of the samples was determined by RBS, while unwanted contaminants such as oxygen and carbon were omitted. In the biased QCM case, deposited mass flux M_b consists only of neutral atoms, to distinguish between the neutral mass flux of aluminium M_{Al} and chromium M_{Cr} following formulas are used:

$$M_{Al} = M_b \frac{C_{b,Al}\, m_{Al}}{C_{b,Al}\, m_{Al} + C_{b,Cr}\, m_{Cr}} \tag{1}$$

$$M_{Cr} = M_b \frac{C_{b,Cr}\, m_{Cr}}{C_{b,Al}\, m_{Al} + C_{b,Cr}\, m_{Cr}} \tag{2}$$

where $C_{b,Al}$ and $C_{b,Cr}$ are relative atomic compositions obtained from EDX and m_{Al} and m_{Cr} are atomic masses. In the unbiased case, the depositing mass flux M_u consists of both neutrals and ions, and to derive the ionic mass flux for aluminium M_{Al^+} and chromium M_{Cr^+} following equations are used:

$$M_{Al^+} = M_u \frac{C_{u,Al}\, m_{Al}}{C_{u,Al}\, m_{Al} + C_{u,Cr}\, m_{Cr}} - M_b \frac{C_{b,Al}\, m_{Al}}{C_{b,Al}\, m_{Al} + C_{b,Cr}\, m_{Cr}} \tag{3}$$

$$M_{Cr^+} = M_u \frac{C_{u,Cr}\, m_{Cr}}{C_{u,Al}\, m_{Al} + C_{u,Cr}\, m_{Cr}} - M_b \frac{C_{b,Cr}\, m_{Cr}}{C_{b,Al}\, m_{Al} + C_{b,Cr}\, m_{Cr}} \tag{4}$$

Then the IMFF can be differentiated between aluminium and chromium as

$$IMFF_{Al} = \frac{M_{Al^+}}{M_{Al^+} + M_{Al}}, \qquad IMFF_{Cr} = \frac{M_{Cr^+}}{M_{Cr^+} + M_{Cr}} \tag{5}$$

To determine the particle fluxes of each element, the mass flux calculated previously is divided by the atomic mass of a given element. This allows for a quantitative comparison of the aluminium and chromium particle fluxes with the argon flux.

Table 2
Properties of investigated target materials [41]. $E_{iz.1}$ and $E_{iz.2}$ denote the first and second ionisation potential of the given material, respectively. The sputter yield for argon (Ar) and self-sputter (SS) yield are obtained from the sputter yield calculator for incident energy of 450 eV [51].

	Al	Cr	Ar
At. mass (amu)	26.98	51.99	39.95
$E_{iz.1}$ (eV)	5.99	6.77	15.76
$E_{iz.2}$ (eV)	18.83	16.49	27.63
Sputter yield (Ar 450 eV)	0.91	1.23	–
Sputter yield (SS 450 eV)	0.88	1.30	–

2.5. Material properties

The properties of the investigated materials – aluminium and chromium – are summarised in Table 2. The table includes sputtering yields collected from a sputter yield calculator from the Surface Physics Group at TU Wien [51], which is based on empirical equations for sputter yields at normal incidence [52]. The sputter yields were calculated for Ar ions as well as target material ions that impinge on the target surface with an energy of 450 eV, in Table 2 denoted as Ar or self-sputtering (SS), respectively.

3. Results and discussion

3.1. Aluminium

Fig. 2(a) shows the particle flux as a function of the applied power at a working pressure of 0.28 Pa using the aluminium cathode. The flux for all investigated particles, i.e., Al atom, Al ion and Ar ion, increases roughly linearly with increasing power in all studied cases. An

increase in both Al ion and Ar ion fluxes can be expected as supplying higher power into the discharge requires higher current densities, which during the measurement increased from 0.3 to 1.3 A·cm^{-2}. As a result, the ionisation probability for all species is higher. Additionally, higher power leads to more particles being sputtered, and thus the flux of Al atoms significantly increases. Note that the atomic flux shows no saturation for higher power, suggesting that the majority of Al atoms are still not ionised near the target. The Ar ion flux is roughly ten times higher than the Al atomic flux and also shows no saturation despite using a fairly low pressure of 0.28 Pa.

The effect of pressure on particle fluxes for the Al target was investigated in the same industrial system for 20 kW of applied power and pressure from 0.28 Pa to 0.96 Pa, which are the limiting pressures for practical use in a given PVD system. The results are depicted in Fig. 2(b), where all three fluxes show roughly constant trends. This observation is in agreement with our previous report [34], in which it was observed that for the standard DCMS cathode at similar power densities, the change in pressure had seemingly no effect on the fluxes. This can be explained by the much higher supply of argon atoms compared to the amount of argon being ionised, even at the lowest investigated pressure. The discharge current determines the ion production rate, and under comparable current conditions, a similar number of argon ions is generated, largely independent of the working pressure. Although not all created ions return to the target due to transport losses, a substantial fraction contributes to sputtering, resulting in comparable sputtered atom fluxes. Additionally, due to working-gas rarefaction [34], transport towards the substrate is only weakly affected by collisions, and similar particle fluxes are therefore observed for all investigated species across the studied pressure range.

An ionised metal flux fraction was calculated as a ratio between the Al ion flux and the sum of Al ion and Al atom fluxes; the result as a function of the applied power is depicted in Fig. 2(c). With power, the IMFF increases linearly from 6% for 5 kW up to about 16% for 25 kW. In the same Fig. 2(c), the IMFF is also depicted for different pressures used in Fig. 2(b) at an applied power of 20 kW. The pressure does not change the IMFF significantly as IMFF is in the range of 12%–15%, which is within the error of the measurement range.

The highest IMFF values observed in this study exceed those reported for laboratory-scale DC magnetron sputtering by an order of magnitude [53–55], yet align with recent measurements in industrial DC magnetron sputtering [36–38]. The IMFF values reported here (6%–16%) are higher than those observed in standard industrial DCMS (2–10%) using a cylindrical rotating cathode under the same working pressure and applied power [36]. Despite using the same target size, in *F*-MS the racetrack area is squeezed to an even smaller area of around 40 cm^2 where the discharge current density reaches up to 1.3 A.cm^{-2}, a value comparable to a lab-scale HiPIMS discharge [32,56]. In comparison, laboratory-scale HiPIMS experiments with aluminium targets at distances of 4 or 8 cm, a pressure of about 0.5 Pa and current density in the range of 0.5–2 A.cm^{-2} have reported IMFF values ranging from 10% to 50% [22,23].

3.2. Chromium

The same set of experiments was conducted using a chromium target, and the results are shown in Fig. 3. The evolution of particle fluxes as a function of applied power at a working pressure of 0.28 Pa is presented in Fig. 3(a). The fluxes of all investigated species – Cr atoms, Cr ions, and Ar ions – increase almost linearly with increasing power in all studied cases.

As shown in Fig. 3(b), variations in pressure do not significantly affect all particle fluxes, for the same reason as in the case of Al sputtering.

Fig. 3(c) illustrates the ionised metal flux fraction for chromium as a function of the applied power. The IMFF increases up to 15 kW, then the increase slows down and seemingly starts to saturate, reaching

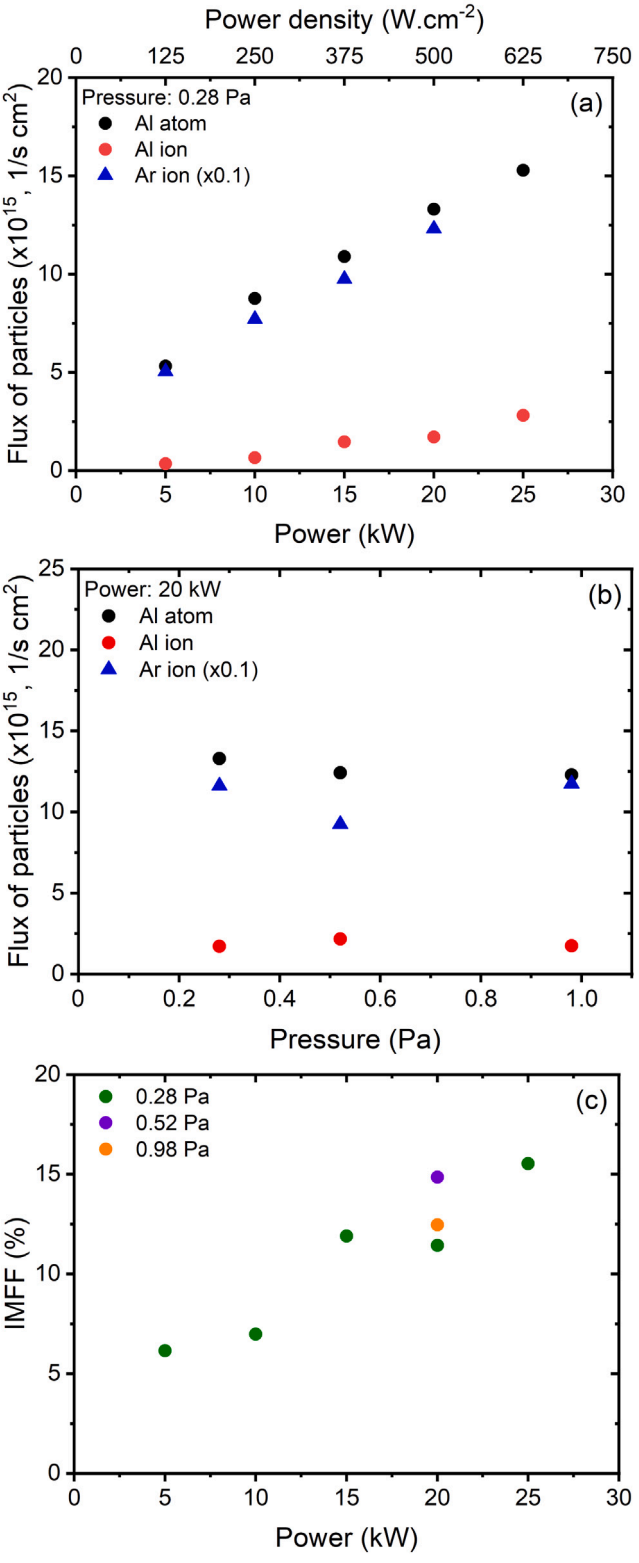

Fig. 2. Flux of aluminium atoms, aluminium ions and argon ions as a function of power at working pressure of 0.28 Pa (a), as a function of pressure for power of 20 kW and ionised metal flux fraction (IMFF) of aluminium as a function of power for different working pressures (c). Note, in figures (a) and (b) the argon ion flux is multiplied by a factor of 0.1 for clear visualisation with other fluxes.

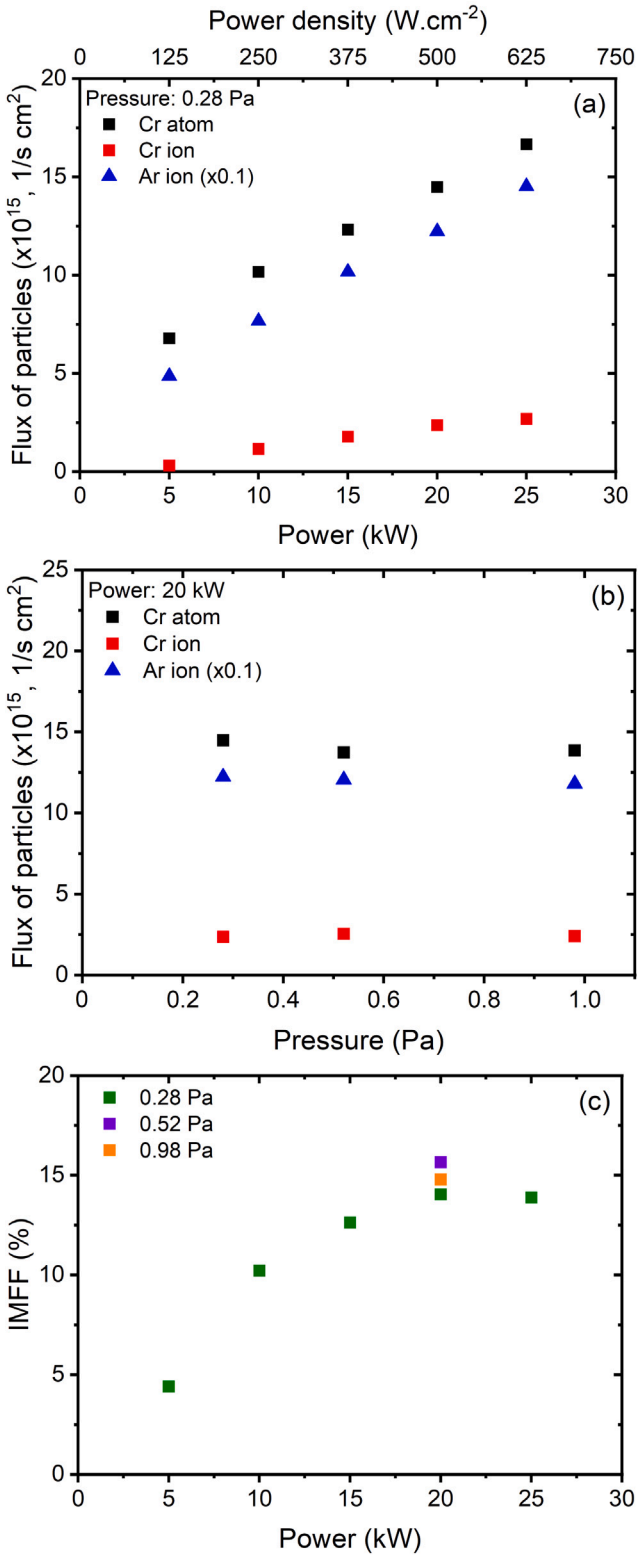

Fig. 3. Flux of chromium atoms, chromium ions and argon ions as a function of power at working pressure of 0.28 Pa (a), as a function of pressure for power of 20 kW and ionised metal flux fraction (IMFF) of chromium as a function of power for different working pressures (c). Note, in figures (a) and (b) the argon ion flux is multiplied by a factor of 0.1 for clear visualisation with other fluxes.

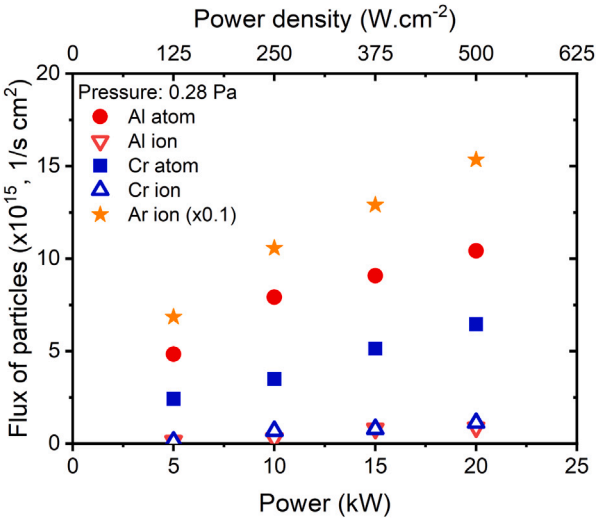

Fig. 4. Flux of aluminium atoms, aluminium ions, chromium atoms, chromium ions and argon ions as a function of power at working pressure of 0.28 Pa for the AlCr (60:40) alloy target. The argon ion flux is multiplied by a factor of 0.1 for better comparison with other fluxes.

approximately 14% at 25 kW. The effect of pressure on IMFF was examined at 20 kW, which revealed no significant variation, as it remained between 14% and 16%, which is within the measurement error.

Compared to standard industrial DCMS [36], the *F*-MS technology achieves higher ionisation also for chromium. In industrial DCMS, only about 5% ionisation was observed at an applied power of 40 kW under a similar working pressure of 0.25 Pa [36].

3.3. AlCr alloy

The same set of experiments as for the pure Al and Cr targets was conducted for the AlCr alloy target (60:40), and the results are shown in Fig. 4. To differentiate between aluminium and chromium fluxes, the procedure using RBS measurement on deposited coatings described in Section 2.4 was used.

Fig. 4 presents the particle fluxes as a function of the supplied power. Moreover, Table 3 summarises fluxes of sputtered species for 20 kW applied power on Al, Cr and AlCr targets for direct comparison. For the compound target, the particle flux of all studied particles increases linearly with an increase in power. Additionally, the ratio between the aluminium and chromium species is roughly identical to the compositional ratio of the target from which they are sputtered. This is consistent with the behaviour of composite targets, where the fluxes of sputtered particles of each element in the target reflect the compositional ratio of the target itself, even when the sputter yields of the individual elements differ. This occurs because the target is sputtered at an atomic level, without mixing the elements [57]. Since the fluxes of sputtered particles reaching the substrate match the target's compositional ratio, it can be inferred that both elements, Al and Cr, were transported to the substrate and scattered by argon in a similar manner. However, it is noteworthy that the overall flux of all particles arriving at the substrate (sum of Al, Al^+, Cr, Cr^+) from the composite target is higher than the corresponding flux from both pure Al and pure Cr targets at the same applied power. This indicates that the sputtering from the composite AlCr target is more efficient than that from the pure Al or Cr targets. This phenomenon, often achieved by adding a heavy element to a target composed of lighter elements, is referred to as sputter amplification [57,58]. Fig. 5 shows the IMFF of aluminium and chromium, calculated from the same results depicted in Fig. 4, as

Table 3
Flux of particles for different Al, Cr and AlCr alloy targets for working pressure of 0.28 Pa and power of 20 kW.

Target	Al atom flux $\times 10^{16}$ s^{-1} cm^{-2}	Al ion flux $\times 10^{15}$ s^{-1} cm^{-2}	Cr atom flux $\times 10^{16}$ s^{-1} cm^{-2}	Cr ion flux $\times 10^{15}$ s^{-1} cm^{-2}	Ar ion flux $\times 10^{17}$ s^{-1} cm^{-2}	Sum of metallic species $\times 10^{16}$ s^{-1} cm^{-2}	Sum of all ions $\times 10^{17}$ s^{-1} cm^{-2}
Aluminium	1.33	1.72	–	–	1.23	1.50	1.25
Chromium	–	–	1.45	2.37	1.22	1.68	1.25
AlCr alloy	1.04	0.87	0.65	1.13	1.53	1.89	1.55

a function of the discharge power for the AlCr alloy. The uncertainty of such a calculation is relatively high (approximately 30%), as it includes compounding contributions from both the subtraction of QCM signals and the multiplications from RBS measurements. Noticeably, points at the 10 kW of power are outliers, mainly induced by the composition measurement. Nevertheless, the results clearly show that the IMFF of chromium is consistently higher than that of aluminium. For both elements, the IMFF increases nearly linearly with power, reaching approximately 15% for Cr and about 8% for Al at 20 kW. The total flux of Ar^+ ions was higher for the alloy target than for the elemental targets, which can be explained by the overall higher discharge current of the alloy target, as shown in Table 1.

These findings highlight a fundamental difference in alloy sputtering, where, despite the fact that a higher amount of aluminium is being sputtered and that aluminium has a lower ionisation potential than chromium, the flux of Al^+ is almost identical to the flux of Cr^+. Also, the data presented here indicate that the IMFF of Al is lower when sputtering from the composite target than from a pure Al target, whereas the IMFF of Cr shows no significant difference between the composite and pure targets. Several mechanisms may contribute to the observed differences in ionisation behaviour. To estimate the residence time of sputtered atoms in the plasma, the mean velocities of Al and Cr atoms leaving the target were calculated using the SDTrimSP [59] simulation code for Al, Cr, and AlCr targets. The calculations show that the velocities of atoms sputtered from the composite target are comparable to those obtained for elemental targets, yielding mean velocities of approximately 7.6 km.s^{-1} for Al and 5.6 km.s^{-1} for Cr. Consequently, aluminium atoms are expected to interact with the magnetised plasma for a shorter time than chromium atoms. However, this difference alone cannot explain the reduced ionisation of aluminium observed for the composite target compared to the pure Al target, as the calculated velocities are essentially unchanged between sputtering of the elemental and composite targets. Further insight can be obtained by considering the electron-impact ionisation rate coefficients, which are available in the literature for Al [60] and Cr [61], both strongly dependent on the electron temperature. Literature [62] also provides experimentally measured electron temperatures during HiPIMS sputtering of elemental Al and Cr targets, indicating a significantly higher electron temperature for Al sputtering (approximately 2.6 eV) than for Cr sputtering (approximately 1.5 eV). Given the similarities in discharge characteristics between *F*-MS and HiPIMS, it is reasonable to assume that the electron temperatures in the *F*-MS experiments with elemental targets are of comparable magnitude, with a higher electron temperature expected for Al target sputtering than for Cr target sputtering. It can be speculated that during sputtering of the AlCr composite target, where Al and Cr atoms coexist in the plasma, chromium atoms cool the electrons more efficiently than aluminium atoms. As a result, the electron temperature during composite AlCr target sputtering is expected to be closer to the value of Cr target sputtering than to that of Al target sputtering. This reduced electron temperature of AlCr target sputtering, compared to sputtering from a pure Al target, leads to a significantly lower ionisation probability of aluminium, which explains the lower IMFF observed for Al during sputtering from the composite target. At the same time, the ionisation conditions for chromium remain similar to those present during sputtering of a pure Cr target, which naturally explains the comparable IMFF values observed for chromium in both cases. For completeness, it should be noted that sputtering

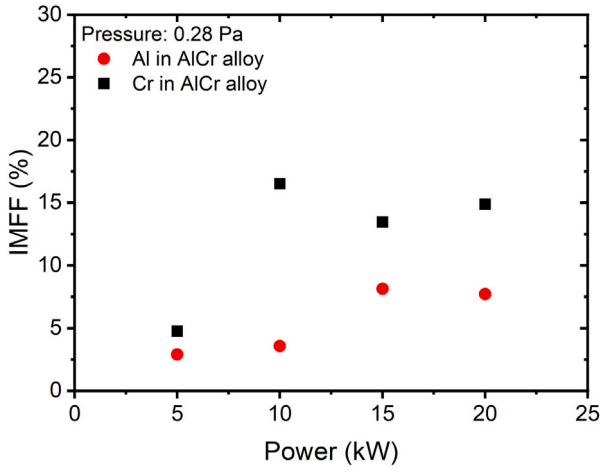

Fig. 5. Ionised metal flux fraction (IMFF) of distinguished Al and Cr ionisation for AlCr alloy discharge as a function of power at working pressure of 0.28 Pa.

from the composite AlCr target was associated with a higher discharge current (54 A) than sputtering from pure Al and Cr targets (45 A and 43 A, respectively), implying a higher electron density in the plasma. Nevertheless, given the strong dependence of the ionisation rate coefficients on the electron temperature, the ionisation probability is expected to be much more strongly influenced by variations in electron temperature than by the moderately increased electron density in the plasma. Consequently, the electron temperature effect is considered to dominate the observed ionisation behaviour.

Based on the present experiment, it is, however, not possible to unambiguously determine which of these effects dominates; the observed behaviour is likely caused by a combination of these, or potentially additional, mechanisms. Moreover, the plasma motion characteristic of *F*-MS technology is not well-suited for detailed diagnostics of the deposition plasma, which further limits the ability to resolve these effects. Nevertheless, the results presented here clearly demonstrate that insights derived from the sputtering of elemental targets cannot be directly transferred to composite targets; the underlying processes differ.

4. Conclusion

This paper quantifies the particle fluxes obtained during the sputtering of pure aluminium and chromium targets, as well as their alloy. A novel measuring approach was utilised, where a biasable QCM system determined the particle flux of film-forming species, and reconnecting the QCM system as a flat Langmuir probe allowed measurement of the argon ion particle flux. For the sputtering of the alloy target, RBS measurements allowed for the differentiation between metallic fluxes of individual metals.

This work provides a comparative analysis of Al, Cr, and AlCr sputtering under industrial *F*-MS magnetron conditions and reveals several fundamental differences between sputtering from elemental and composite targets. The total sputtered particle flux measured for the alloy target was higher than the fluxes determined for both pure Al and

pure Cr targets, and the fluxes of individual species (Al and Cr) from the alloy target closely followed the elemental composition of the target itself. This demonstrates that the relative contributions of Al and Cr to the total particle flux are preserved during alloy sputtering, indicating that the sputter amplification effect is occurring.

Clear differences in ionisation behaviour were observed: the IMFF of Al was substantially lower when sputtering from the alloy target than from the pure Al target, while the IMFF of Cr remained essentially unchanged between the alloy and pure Cr targets. These findings show that the ionisation of sputtered species during alloy sputtering does not simply replicate the behaviour known from elemental targets. Several mechanisms may contribute to the altered ionisation dynamics, including a shift of the Al ionisation zone closer to the target surface, leading to increased back-attraction, modifications of electron temperature due to the simultaneous presence of Al and Cr atoms in the plasma, or differences in initial sputtering velocities affecting residence times in the magnetised plasma. Although the present experiment cannot identify which of these mechanisms is dominant, the observed trends are likely caused by a combination of these effects. Across all measurements, Ar^+ remained the primary ion bombarding the substrate, indicating that it is the main driving force influencing the film growth. Moreover, the total Ar^+ ion flux was higher for the compound target than for the elemental targets, which was ascribed to the higher discharge current using the compound target.

CRediT authorship contribution statement

Peter Klein: Writing – review & editing, Writing – original draft, Visualization, Validation, Methodology, Investigation, Formal analysis, Data curation, Conceptualization. **Jaroslav Hnilica:** Writing – review & editing, Writing – original draft, Visualization, Validation, Investigation, Formal analysis, Data curation. **Mojmír Jílek:** Writing – review & editing, Resources, Project administration, Methodology, Conceptualization. **Mayur Khan:** Investigation, Formal analysis, Data curation. **Anna Macková:** Writing – review & editing, Validation, Supervision, Resources, Project administration, Methodology, Funding acquisition. **Petr Vašina:** Writing – review & editing, Writing – original draft, Validation, Supervision, Resources, Project administration, Funding acquisition, Conceptualization.

Declaration of competing interest

The authors declare that they have no known competing financial interests or personal relationships that could have appeared to influence the work reported in this paper.

Acknowledgements

This research was supported by the project LM2023039 funded by the Ministry of Education, Youth and Sports of the Czech Republic. Measurements of the chemical composition of the coatings were carried out at the CANAM infrastructure of the NPI ASCR Rez, supported through the MEYS project No. LM2015056. The author A. M. acknowledges the assistance provided by the Ferroic Multifunctionalities project, supported by the Ministry of Education, Youth, and Sports of the Czech Republic. Project No. CZ.02.01.01/00/22_008/0004591, co-funded by the European Union.

Data availability

Data will be made available on request.

References

[1] J. Pawel, C. McHargue, J. Wert, The influence of ion bombardment on the adhesion of thin films to substrates, Nucl. Instrum. Methods Phys. Res. Sect. B: Beam Interact. Mater. Atoms 46 (1–4) (1990) 392–396.
[2] M. Samuelsson, D. Lundin, J. Jensen, M.A. Raadu, J.T. Gudmundsson, U. Helmersson, On the film density using high power impulse magnetron sputtering, Surf. Coat. Technol. 205 (2) (2010) 591–596.
[3] P. Souček, J. Hnilica, P. Klein, M. Fekete, P. Vašina, Microstructure of titanium coatings controlled by pulse sequence in multipulse HiPIMS, Surf. Coat. Technol. 423 (2021) 127624.
[4] D. Xie, L. Wei, H. Liu, K. Zhang, Y. Leng, D. Matthews, R. Ganesan, Y. Su, Deposition of titanium films on complex bowl-shaped workpieces using DCMS and HiPIMS, Surf. Coat. Technol. 442 (2022) 128192.
[5] P. Souček, T. Schmidtová, L. Zábranský, V. Buršíková, P. Vašina, O. Caha, J. Buršík, V. Peřina, R. Mikšová, Y. Pei, J. De Hosson, On the control of deposition process for enhanced mechanical properties of nc-TiC/aC: H coatings with DC magnetron sputtering at low or high ion flux, Surf. Coat. Technol. 255 (2014) 8–14.
[6] V. Tiron, I.-L. Velicu, D. Cristea, N. Lupu, G. Stoian, D. Munteanu, Influence of ion-to-neutral flux ratio on the mechanical and tribological properties of TiN coatings deposited by HiPIMS, Surf. Coat. Technol. 352 (2018) 690–698.
[7] S. Konstantinidis, A. Hemberg, J. Dauchot, M. Hecq, Deposition of zinc oxide layers by high-power impulse magnetron sputtering, J. Vac. Sci. Technol. B: Microelectron. Nanometer Struct. Process. Meas. Phenom. 25 (3) (2007) L19–L21.
[8] K. Bobzin, N. Bagcivan, P. Immich, S. Bolz, J. Alami, R. Cremer, Advantages of nanocomposite coatings deposited by high power pulse magnetron sputtering technology, J. Mater. Process. Technol. 209 (1) (2009) 165–170.
[9] F. Magnus, A.S. Ingason, O. Sveinsson, S. Olafsson, J. Gudmundsson, Morphology of TiN thin films grown on SiO2 by reactive high power impulse magnetron sputtering, Thin Solid Films 520 (5) (2011) 1621–1624.
[10] I. Petrov, L. Hultman, U. Helmersson, J.-E. Sundgren, J. Greene, Microstructure modification of TiN by ion bombardment during reactive sputter deposition, Thin Solid Films 169 (2) (1989) 299–314.
[11] A. Amin, D. Köhl, M. Wuttig, The role of energetic ion bombardment during growth of TiO2 thin films by reactive sputtering, J. Phys. D: Appl. Phys. 43 (40) (2010) 405303.
[12] F. Cemin, G. Abadias, T. Minea, C. Furgeaud, F. Brisset, D. Solas, D. Lundin, Benefits of energetic ion bombardment for tailoring stress and microstructural evolution during growth of Cu thin films, Acta Mater. 141 (2017) 120–130.
[13] G. Abadias, E. Chason, J. Keckes, M. Sebastiani, G.B. Thompson, E. Barthel, G.L. Doll, C.E. Murray, C.H. Stoessel, L. Martinu, Stress in thin films and coatings: Current status, challenges, and prospects, J. Vac. Sci. Technol. A 36 (2) (2018).
[14] G. Greczynski, S. Mráz, J. Schneider, L. Hultman, Metal-ion subplantation: A game changer for controlling nanostructure and phase formation during film growth by physical vapor deposition, J. Appl. Phys. 127 (18) (2020).
[15] J. Paulitsch, M. Schenkel, T. Zufraß, P.H. Mayrhofer, W.-D. Münz, Structure and properties of high power impulse magnetron sputtering and DC magnetron sputtering CrN and TiN films deposited in an industrial scale unit, Thin Solid Films 518 (19) (2010) 5558–5564.
[16] P. Souček, J. Daniel, J. Hnilica, K. Bernátová, L. Zábranský, V. Buršíková, M. Stupavská, P. Vašina, Superhard nanocomposite nc-TiC/aC: H coatings: The effect of HiPIMS on coating microstructure and mechanical properties, Surf. Coat. Technol. 311 (2017) 257–267.
[17] H. Larhlimi, O. Abegunde, Y. Samih, A. Ghailane, M. Makha, J. Alami, Effect of carbon content on the structural, mechanical and corrosion properties of TiC films deposited using a HiPIMS discharge, Surf. Coat. Technol. 451 (2022) 129028.
[18] J. Vlček, D. Kolenatý, J. Houška, T. Kozák, R. Čerstvý, Controlled reactive HiPIMS—effective technique for low-temperature (300 C) synthesis of VO2 films with semiconductor-to-metal transition, J. Phys. D: Appl. Phys. 50 (38) (2017) 38LT01.
[19] V. Tiron, I.-L. Velicu, T. Matei, D. Cristea, L. Cunha, G. Stoian, Ultra-short pulse HiPIMS: A strategy to suppress arcing during reactive deposition of SiO2 thin films with enhanced mechanical and optical properties, Coatings 10 (7) (2020) 633.
[20] J.-R. Tsai, P.-C. Juan, P.-J. Chen, Characteristics of metal-gate metal-insulator-semiconductor capacitor with ZrN capping layer fabricated by high-power impulse magnetron sputtering, Thin Solid Films 618 (2016) 55–59.
[21] Z. Hubička, M. Zlamal, J. Olejníček, D. Tvarog, M. Čada, J. Krýsa, Semiconducting p-type copper iron oxide thin films deposited by hybrid reactive-HiPIMS+ ECWR and reactive-HiPIMS magnetron plasma system, Coatings 10 (3) (2020) 232.
[22] B. DeKoven, P. Ward, R. Weiss, D. Christie, R. Scholl, W. Sproul, F. Tomasel, A. Anders, Carbon thin film deposition using high power pulsed magnetron sputtering, in: Proceedings of the 2003 Annual Technical Meeting of the Society of Vacuum Coaters, SVC- Society of Vacuum Coaters, Albuquerque, NM, 2003, URL: https://www.osti.gov/biblio/877319.

[23] D. Lundin, M. Čada, Z. Hubička, Ionization of sputtered Ti, Al, and C coupled with plasma characterization in HiPIMS, Plasma Sources Sci. Technol. 24 (3) (2015) 035018.

[24] L. Meng, H. Yu, M.M. Szott, J.T. McLain, D.N. Ruzic, Downstream plasma transport and metal ionization in a high-powered pulsed-plasma magnetron, J. Appl. Phys. 115 (22) (2014).

[25] J. McLain, P. Raman, D. Patel, R. Spreadbury, J. Uhlig, I. Shchelkanov, D. Ruzic, Linear magnetron HiPIMS high deposition rate magnet pack, Vacuum 155 (2018) 559–565.

[26] J. Fischer, M. Renner, J.T. Gudmundsson, M. Rudolph, H. Hajihoseini, N. Brenning, D. Lundin, Insights into the copper HiPIMS discharge: deposition rate and ionised flux fraction, Plasma Sources Sci. Technol. 32 (12) (2023) 125006.

[27] V. Semenov, E. Oks, A. Solovyev, M. Shandrikov, Ionization of copper in gas and gasless modes of continuous high-power magnetron sputtering, Vacuum 230 (2024) 113649.

[28] B. Biskup, C. Maszl, W. Breilmann, J. Held, M. Böke, J. Benedikt, A. Von Keudell, Influence of spokes on the ionized metal flux fraction in chromium high power impulse magnetron sputtering, J. Phys. D: Appl. Phys. 51 (11) (2018) 115201.

[29] Z. Hubička, Š. Kment, J. Olejníček, M. Čada, T. Kubart, M. Brunclíková, P. Kšírová, P. Adámek, Z. Remeš, Deposition of hematite Fe2O3 thin film by DC pulsed magnetron and DC pulsed hollow cathode sputtering system, Thin Solid Films 549 (2013) 184–191.

[30] T. Kubart, M. Čada, D. Lundin, Z. Hubička, Investigation of ionized metal flux fraction in HiPIMS discharges with Ti and Ni targets, Surf. Coat. Technol. 238 (2014) 152–157.

[31] P. Poolcharuansin, M. Bowes, T.J. Petty, J.W. Bradley, Ionized metal flux fraction measurements in HiPIMS discharges, J. Phys. D: Appl. Phys. 45 (32) (2012) 322001.

[32] T. Shimizu, M. Zanáška, R. Villoan, N. Brenning, U. Helmersson, D. Lundin, Experimental verification of deposition rate increase, with maintained high ionized flux fraction, by shortening the HiPIMS pulse, Plasma Sources Sci. Technol. 30 (4) (2021) 045006.

[33] A. Kapran, C. Ballage, Z. Hubička, T. Minea, 2D analysis of sputtered species transport in high-power impulse magnetron sputtering (HiPIMS) discharge, J. Appl. Phys. 135 (17) (2024).

[34] J. Hnilica, P. Souček, M. Ondryáš, P. Klein, M. Fekete, P. Vašina, Exploring different approaches of multipulse HiPIMS, Surf. Coat. Technol. 496 (2025) 131670.

[35] M. Ondryáš, P. Klein, J. Hnilica, P. Vašina, Quantifying argon and metal ion fluxes in HiPIMS using a biasable QCM, Surf. Coat. Technol. 517 (2025) 132847.

[36] P. Klein, J. Hnilica, V. Sochora, P. Vašina, Exploring ionised metal flux fraction in magnetron sputtering: Insights from laboratory and industrial applications, Surf. Coat. Technol. 500 (2025) 131866.

[37] P. Klein, J. Hnilica, V. Sochora, P. Souček, M. Fekete, P. Vašina, Enhancement of ionized metal flux fraction without compromising deposition rate in industrial magnetron sputtering, Surf. Coat. Technol. 489 (2024) 131142.

[38] J. Hnilica, P. Klein, M. Učík, S. Debnárová, J. Klusoň, P. Vašina, On direct-current magnetron sputtering at industrial conditions with high ionization fraction of sputtered species, Surf. Coat. Technol. 487 (2024) 131028.

[39] R.A. Powell, S.M. Rossnagel, PVD for microelectronics: Sputter deposition applied to semiconductor manufacturing, Academic Press, San Diego, 1999.

[40] D. Depla, Sputter deposition with powder targets: An overview, Vacuum 184 (2021) 109892.

[41] D. Siderius, NIST Standard Reference Simulation Website - SRD 173, [Online]. Available: https://doi.org/10.18434/mds2-232 (Accessed 1 November 2024), National Institute of Standards and Technology.

[42] D. Christie, Target material pathways model for high power pulsed magnetron sputtering, J. Vac. Sci. Technol. A: Vac. Surfaces, Films 23 (2) (2005) 330–335.

[43] J. Čapek, M. Hála, O. Zabeida, J.-E. Klemberg-Sapieha, L. Martinu, Deposition rate enhancement in HiPIMS without compromising the ionized fraction of the deposition flux, J. Phys. D: Appl. Phys. 46 (20) (2013) 205205.

[44] SHM, s.r.o., Šumperk, Czech Republic [link], URL: https://shm-cz.cz/en/.

[45] F.F. Klimashin, J. Klusoň, M. Učík, R. Žemlička, M. Jílek, A. Lümkemann, J. Michler, T.E.J. Edwards, High-power-density sputtering of industrial-scale targets: Case study of (Al, Cr) N, Mater. Des. 237 (2024) 112553.

[46] R. De Gryse, J. Haemers, W. Leroy, D. Depla, Thirty years of rotatable magnetrons, Thin Solid Films 520 (18) (2012) 5833–5845.

[47] L. Wu, E. Ko, A. Dulkin, K.J. Park, S. Fields, K. Leeser, L. Meng, D.N. Ruzic, Flux and energy analysis of species in hollow cathode magnetron ionized physical vapor deposition of copper, Rev. Sci. Instrum. 81 (12) (2010) 123502.

[48] P. Kudláček, J. Vlček, K. Burcalová, J. Lukáš, Highly ionized fluxes of sputtered titanium atoms in high-power pulsed magnetron discharges, Plasma Sources Sci. Technol. 17 (2) (2008) 025010.

[49] W. Fang, J. Chen, F. Cai, Z. Chai, F. Ba, Surface stress release in AlCrN coatings determined by synchrotron radiation multi-reflection grazing-incidence X-ray diffraction, Thin Solid Films 787 (2023) 140142.

[50] F. Ferreira, C. Sousa, A. Cavaleiro, A. Anders, J. Oliveira, Phase tailoring of tantalum thin films deposited in deep oscillation magnetron sputtering mode, Surf. Coat. Technol. 314 (2017) 97–104.

[51] Surface Physics Group at T.U. Wien, [Online]. Available: https://www2.iap.tuwien.ac.at/www/surface/sputteryield (Accessed 21 March 2025).

[52] N. Matsunami, Y. Yamamura, Y. Itikawa, N. Itoh, Y. Kazumata, S. Miyagawa, K. Morita, R. Shimizu, H. Tawara, Energy Dependence of the Yields of Ion-Induced Sputtering of Monatomic Solids, Technical Report, 1983.

[53] I. Petrov, A. Myers, J. Greene, J. Abelson, Mass and energy resolved detection of ions and neutral sputtered species incident at the substrate during reactive magnetron sputtering of Ti in mixed Ar+ N2 mixtures, J. Vac. Sci. Technol. A: Vac. Surfaces, Films 12 (5) (1994) 2846–2854.

[54] P. Vašina, M. Fekete, J. Hnilica, P. Klein, L. Dosoudilová, P. Dvořák, Z. Navrátil, Determination of titanium atom and ion densities in sputter deposition plasmas by optical emission spectroscopy, Plasma Sources Sci. Technol. 24 (6) (2015) 065022.

[55] A. Solovyev, V. Oskirko, V. Semenov, K. Oskomov, S. Rabotkin, Comparative study of Cu films prepared by DC, high-power pulsed and burst magnetron sputtering, J. Electron. Mater. 45 (8) (2016) 4052–4060.

[56] H. Hajihoseini, M. Čada, Z. Hubička, S. Ünaldi, M.A. Raadu, N. Brenning, J.T. Gudmundsson, D. Lundin, The effect of magnetic field strength and geometry on the deposition rate and ionized flux fraction in the HiPIMS discharge, Plasma 2 (2) (2019) 201–221.

[57] H.M. Urbassek, M.L. Nietiadi, R.M. Bradley, G. Hobler, Sputtering of Si_cGe_{1-c} nanospheres, Phys. Rev. B 97 (2018) 155408.

[58] S. Berg, A.M. Barklund, B. Gelin, C. Nender, I. Katardjiev, Atom assisted sputtering yield amplification, J. Vac. Sci. Technol. A 10 (4) (1992) 1592–1596.

[59] A. Mutzke, R. Schneider, W. Eckstein, R. Dohmen, K. Schmid, U. von Toussaint, G. Bandelow, *SDTrimSP Version 6.00 (IPP Report 2019-02)*. Garching: Max-Planck-Institut für Plasmaphysik, 2019.

[60] M.A. Raadu, I. Axnäs, J.T. Gudmundsson, C. Huo, N. Brenning, An ionization region model for high-power impulse magnetron sputtering discharges, Plasma Sources Sci. Technol. 20 (6) (2011) 065007.

[61] J. Gao, F. Ferreira, M. Lei, Global model on oscillation discharge characteristics during deep oscillation magnetron sputtering of Cr target, J. Appl. Phys. 132 (20) (2022) 203303.

[62] J. Held, V. Schulz-von der Gathen, A. von Keudell, Ionization of sputtered material in high power impulse magnetron sputtering plasmas—comparison of titanium, chromium and aluminum, Plasma Sources Sci. Technol. 32 (6) (2023) 065006.